2

Conf-9408127--3

UCRL-JC-115189
PREPRINT

Ablative Stabilization of the Rayleigh-Taylor Instability in Regimes Relevant to Inertial Confinement Fusion

J. D. Kilkenny

This paper was prepared for inclusion in a book collection from the
Scottish Universities Summer School in Physics
St. Andrews, Scotland
August 7-12, 1994

August 4, 1994

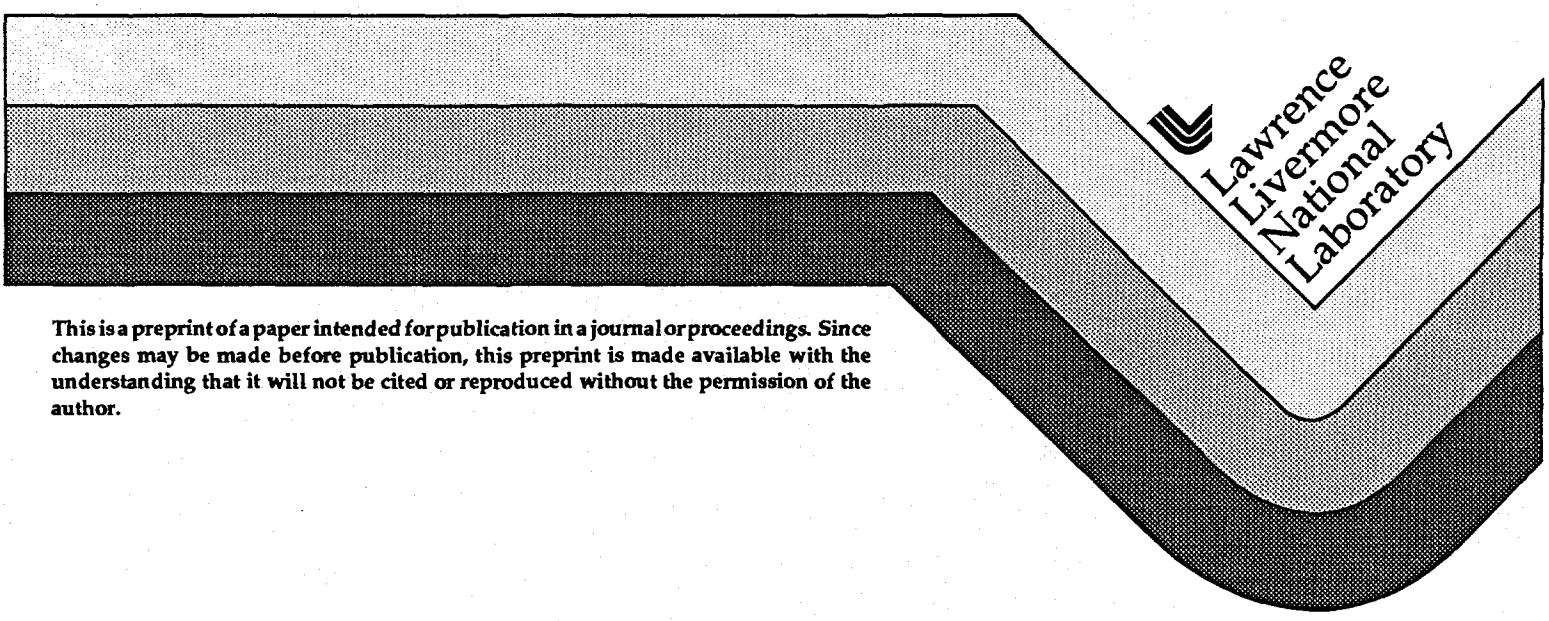

Lecture 3 : Ablative stabilization of the Rayleigh-Taylor instability in regimes relevant to Inertial Confinement Fusion

In this lecture, we go into the fundamentals of the Rayleigh-Taylor instability and the experimental measurements that show it is stabilized sufficiently by ablation in regimes relevant to ICF.

3.1 Introduction

As shown in an accompanying lecture an ablatively imploded shell is hydrodynamically unstable, the dominant instability being the well known Rayleigh-Taylor[1] instability with growth rate

$$\gamma = \sqrt{Akg}$$

Where $k=2\pi / \lambda$ is the wave number, g is the acceleration and A the Attwood number $(\rho_{hi} - \rho_{lo}) / (\rho_{hi} + \rho_{lo})$. where ρ_{hi} is the density of the heavier fluid and ρ_{lo} is the density of the lighter fluid. A theoretical understanding of ablative stabilization has gradually evolved, confirmed over the last five years by experiments. The linear growth is very well understood with excellent agreement between experiment and simulation for planar geometry with wavelengths in the region of 30-100μm. There is an accurate, albeit phenomenological dispersion relation. The non-linear growth has been measured and agrees with calculations.

The R-T instability of a heavy fluid (ρ_{hi}) supported by a lighter fluid (ρ_{lo}) in a gravitational field is analogous to a compound pendulum with a heavier mass on top as illustrated in Fig. 1. For incompressible fluids, periodicity in x forces the eigenmodes of the surface wave to have the form

$$\sim \cos kx \; e^{-kz} \qquad 1$$

Close to the interface the fluid flow lines resemble the manometer illustrated in the center of Fig 1. The stability of the manometer is simply modeled by the compound pendulum on the right with uneven "masses" ρ_{hi} and ρ_{lo}. The angular motion of the pendulum is given by

$$(\rho_{hi} - \rho_{lo}) \frac{g\lambda}{2\pi} \theta = (\rho_{hi} + \rho_{lo}) \left(\frac{\lambda}{2\pi}\right)^2 \ddot{\theta}$$

with a growth rate γ for θ of

$$\gamma^2 = \frac{\rho_{hi}-\rho_{lo}}{\rho_{hi}+\rho_{lo}} .gk \qquad 2$$

or $\gamma = \sqrt{Agk}$. This model demonstrates the $k^{1/2}$ growth rate and how A, the Attwood number, arises. The numerator in Eq. (2) results from the torque on the

pendulum , proportional to the difference in the masses, whereas the denominator represents the inertia, proportional to the sum of the masses.

In the classical growth of the interface non-linearity starts when the amplitude of the perturbation is no longer negligible compared to its wavelength,[3] that is, $a \sim \lambda/10$. At this point, more rapidly growing harmonics appear, transforming a sinusoidal perturbation to a characteristic bubble and spike. Surface tension and viscosity stabilize the R-T instability at short wavelengths[4].

For ICF, the low density, high pressure ablating plasma accelerates the high density shell and so $\rho_{lo} << \rho_{hi}$ and the Attwood number is close to unity. Here the density gradient can have a stabilizing effect that can be explained via an effective Attwood number. The perturbation extends into the fluid a characteristic distance e^{-kz}. If the scale length for density gradients is $L = \rho/\nabla\rho$, the density change the perturbation "sees" is reduced by e^{-kL}. For $kL << 1$ this can be approximated by $A \rightarrow 1/1+kL$, giving $\gamma = [gk/(1+kL)]^{1/2}$. In the limit $kL >> 1$ this form goes to $\gamma^2 = g/L$

The R-T instability is ubiquitous in science. Aside from fluids, it appears in astrophysics[5], geophysics[6] and nuclear physics[7]. It is also well known to occur in magnetically contained plasmas. For example in a magnetically contained z-pinch, the outer surface is R-T unstable when the (low density) magnetic field inwardly accelerates the (high density) plasma column. Surface waves grow, but because of the relatively low density, viscosity plays a stabilizing role for surface waves[8].

The Richtmeyer-Meshkov (R-M) instability is the R-T analog for impulsive acceleration. The Kelvin-Helmholtz (K-H) instability grows from shear across an interface. Experiments on both types of instabilities have been performed on the Nova laser and are reported elsewhere[9,10].

Although the ablation front instability is the primary hydrodynamic instability of an implosion, it is not the only instability, as illustrated in Fig. 2. The ablation front instability amplifies outer surface finish imperfections, (or laser seeded modulations) of effective amplitude $a_0(0)$ by a growth factor GF_0. This amplification occurs for a distance $\sim R_0/2$, during the inwards acceleration. The

amplified outer surface perturbations a_o then feed through to provide inner surface perturbations of amplitude $a_i(0)$ according to $a_i(0) = a_0 \cdot FT$, where FT is a shell feed through factor.

In the final phase of the implosion, when the shell is decelerated by the laser density but higher pressure fuel, the inner surface perturbations are R-T unstable with a growth factor GF_i given by $a_i = a_i(0)\ GF_i$. As an approximation

$$a_i \sim a_o(0) \cdot GF_o \cdot FT \cdot GF_i$$

In ICF a high aspect ratio shell is required to amplify the ablation pressure. If a shell of in-flight thickness ΔR is uniformly accelerated at g from its initial radius R_0, to $R_0/2$ by an ablation pressure P_A, its velocity is

$$v_{sh}^2 = 2g\ R_0/2 = [P_A/(\rho \Delta R)]\ R_0$$

The shell then compresses the fuel to a final pressure P_F a lower limit that ignores further convergence effects is given approximately by the "Bernoulli pressure" $\rho_{sh} v_{sh}^2$ of the shell, i.e.,

$$P_F \sim \rho_{sh} v_{sh}^2 = P_A \left(\frac{R_0}{\Delta R}\right)$$

However surface imperfections grow because of the Rayleigh-Taylor instability, and place an upper limit on the in-flight aspect ratio.

The outer surface of a shell is R-T unstable during the ablative acceleration, as inward acceleration is equivalent to outward g. In the accelerating reference frame of the ablation front, the heavy shell fluid is "sitting on top of" the hot, low density ablation fluid. The most damaging modes are those wavelengths that can most easily cause the shell to break up. These modes have wave number $k \sim 2\pi/\Delta R$[11,12] although there is uncertainty at the factor of two level. Longer wavelengths grow too slowly and shorter wavelength modes saturate. For simplicity, assume a single mode $k=2\pi/\Delta R$, constant acceleration from R_0 to $R_0/2$, and a growth rate of $\gamma=\varepsilon(kg)^{1/2}$, where ε is a reduction factor from the classical growth rate. The number of e-foldings can then be written as

$$n = \int \gamma\ dt \sim \varepsilon \left(2\pi \frac{R_0}{\Delta R}\right)^{1/2}$$

The outer surface finish $a_o(0)$ of a shell depends on the shell material and for envisaged ablators will be no better than $a_o(0) \sim 250$Å. There will be enhanced cooling of the fuel when the size of the perturbations becomes a significant fraction of the radius of the compressed fuel that is after growth to $a_o \sim 10$ μm, the maximum growth factor at the outer surface (GFo) would be e^6 (~400), i.e., $n \leq 6$. The maximum in-flight aspect ratio that can be used to keep $n < 6$ is given by

$$\frac{R_0}{\Delta R} = \frac{1}{2\pi}\left(\frac{n}{\varepsilon}\right)^2 < \frac{36}{2\pi\varepsilon^2}$$

This startling fact, a shell that is classically Rayleigh-Taylor unstable ($\varepsilon=1$) can only be accelerated over 6 times its initial thickness before surface perturbations grow sufficiently to break up the shell, has focused the attention of ICF scientists on hydrodynamic instabilities. ICF depends crucially on an accurate knowledge of the growth rates of hydrodynamic instabilities. Typically, designs require $R_0/\Delta R$ in the range 25-50, implying

$$\varepsilon = \frac{\gamma}{\sqrt{kg}} < 0.5$$

Other factors complicate this simplistic view and a more rigorous model is presented in reference[13], where a spectrum of wave numbers is used.

3.2 The ablative stabilization of the R-T growth rate

A simple "burning in" argument, accredited to Lindl, and based on numerical work, makes ablative stabilization reasonable. The amplitudes of the R-T eigenfunctions decay exponentially into the higher density material as e^{-kz}, with a temporal growth of $e^{\gamma_c t}$, where $\gamma^2_c = kg$. After some time, the perturbation has grown by a factor $e^{\gamma_c \Delta t}$. However if there is flow at velocity v_A across the interface, the interface effectively moves a distance $v_A\Delta t$ into the fluid and samples an eigenfunction smaller by a factor $e^{-kv_A\Delta t}$. The net growth factor at the ablation surface is $e^{\gamma_c \Delta t - kv_A\Delta t}$. Hence, the net growth rate is

$$\gamma = (kg)^{1/2} - kv_A \qquad 3$$

More rigorous analytic and numerical studies have examined the growth rate, generally finding a reduction associated with a flow of material through the unstable region and with "fire-polishing"[14] of the perturbations. Early two dimensional simulations[11] also found the growth rate of the Rayleigh-Taylor instability to be smaller than $\sqrt{kg}$.

From analytic work various formulae have been proposed. Bodner[15] derived

$$\gamma \sim (kg + 0.25k^2v_A^2)^{1/2} - 0.5kv_A$$

for kL =1 for a semi-analytic model and a more familiar appearing dispersion relation

$$\gamma = (kg)^{1/2} - kv_A$$

for kL infinite (that is, stabilization due to convection only).

Boris[(2)] fit a dispersion relation to numerical solutions and proposed

$$\gamma^2 = kg/(1 + kL) - 1.33k^2gL$$

At LLNL in the early eighties[16,] Lindl fit numerical simulations for x-ray drive and proposed a physically reasonable formula

$$\gamma = [kg/(1+kL)]^{1/2} - kv_A.$$

More recent analytic work by Betti[17] has produced

$$\gamma = [Akg/(1+(4/9)\ AkL)]^{1/2} - 1.5\ kv_A.$$

The most widely accepted dispersion relation is from Takabe[18]

$$\gamma = 0.9\ (kg)^{1/2} - 3kv_A$$

for direct drive with kL << 1. Takabe For direct drive the density scale length L, is usually short so that kL<<1 for relevant values of k. To allow for density gradients a modified form of the Takabe relation is

$$\gamma = [kg/(1+kL)]^{1/2} - 3\,k\,v_A \qquad 4$$

Why is the coefficient of the ablative stabilization term $3\cdot(kv_A)$ and not $1\cdot(kv_A)$ as would be expected from the simple "burning in" argument? Examination of the flow profiles from a calculation gives some insight. Fig. 3 shows calculations of the density and pressure profiles for 0.26 μm laser acceleration of a plastic foil at $2\,10^{14}$ W/cm^2. The R-T unstable regime, where $\nabla p.\nabla\rho$ is negative, is also shown. The flow has

$$\rho\, v = \dot{M} = \text{constant}$$

as there is little change in radius. Here, v and $\dot{M}$ correspond to the flow velocity and mass ablation rate per unit area. In the R-T unstable region ρ varies rapidly and the velocity therefore varies rapidly. The ablation velocity v_A in the Takabe formula, eq. 4, is defined as the material flow velocity at the maximum of ρ. However, the most appropriate velocity for the "burning in" argument is the average velocity in the unstable region, which for the particular case of Fig. 3 is 2-3 v_A. It is therefore reasonable that β ~2-3.

The flow velocity varies significantly in space and so a more useful form of the modified Takabe relation is

$$\gamma = (kg/(1+kL))^{1/2} - 3k\dot{M}/\rho_{max} \qquad 5$$

as $\rho\, v = \dot{M}$ and $\dot{M}$ is a good constant of the flow.

In the mid-eighties there was disagreement over the degree of ablative stabilization, with disputes over the accuracy of zoning in calculations[19] and the efficacy of stabilization at shorter laser wavelengths. Recently, calculations[19,20] of the direct drive ablation front R-T instability have shown agreement with one

another. For direct drive, without radiation effects, the Takabe formula is found to be an excellent approximation. Fig 4 (left) shows normalized values of $\gamma / \sqrt{gk}$ from references 19 & 20, for direct drive without preconditioning the foil. There is reasonable agreement between the calculations from the two different codes, although there is inadequate ($\gamma / \sqrt{gk} > 0.5$) stabilization for all significant wavelengths. However from Eq. (5) if ρ_{max} is decreased, by artificially raising the initial isentrope of the calculation, $\dot{M}$ stays virtually the same and an increased level of ablative stabilization results, also as shown on Fig. 4 (left).

There is a price to be paid for the increased stabilization. Going to a higher isentrope lowers $\rho_{sh} v_{sh}^2$ and therefore the final fuel pressure (see Sec. II). Calculations[21] show that increasing the isentrope is effective for direct drive ICF at the MJ level as long as $\alpha < 4$, where $\alpha = \frac{P}{P_{Fermi}}$ and P_{Fermi} is the Fermi degenerate pressure, and P is the pressure in the shell.

Figure 4 (right) also shows the calculated stabilization factor $\varepsilon = \gamma / \sqrt{gk}$ for x-ray drive[22]. For the x-ray drive, there is clearly adequate stabilization without artifically increasing the isotope for wavelengths with $\lambda \sim 50\mu m$, that is $\gamma / \sqrt{gk} < 0.5$. The major reason for the greater R-T reduction for x-ray drive is that the mass ablation rate for x-ray drive ($\dot{M}$ in eq. 5) is several times larger than for direct drive. Additionally, x-ray drive produces a higher ablation pressure, lowering the required pressure amplificiation.

3.3 Experimental Techniques

There are two main techniques for measuring the growth of Rayleigh-Taylor instabilities as shown in Fig. 5. Side-on radiography[23], although the most graphic, suffers from system difficulties. In emulating ignition capsules with planar experiments, large growth factors at the outer surface $GF_o \sim 100$, are required. Modulations start to saturate at $a_o \sim \lambda / 10$, which for $\lambda \sim 50\ \mu$ m requires a spatial resolution $< 5\ \mu m$, better than is realized on large laser systems[24]. Even if spatial resolution improvements were possible, motional blurring and the need to keep in-flight packages planar, would restrict the utility of side-on radiography.

The most successful technique for accurate measurements of R-T growth is face-on radiography 25 as shown in Fig. 5. In contrast to side-on radiography, the restriction on spatial resolution is the wavelength of the perturbation. The temporal resolution and planarity requirements are relaxed. The only significant disadvantage of face-on radiography is that modulations of areal density, not perturbation amplitude, are measured. An important advantage of face-on radiography is that as long as Kelvin-Helmholtz roll-over does not occur, face on radiography can adequately measure bubble and spike formation.

Other techniques for measuring R-T growth have used x-ray spectroscopy to search for premature emission from a buried tracer layer, indicating enhanced burn through due to RT-induced mixing. Semi-quantitative results have been achieved with this technique,[26] both in planar and in convergent geometry.

3.4 X-ray driven planar package experiments

X-ray driven planar hydrodynamic instability experiments have been performed on Nova [22,27,28] and the Vulcan laser[29]. X-ray drive has a larger ablative stabilization because the mass ablation rate is higher for x-ray drive than laser drive at the same incident flux and from Eq. (5) directly leads to R-T growth rates for x-ray drive being significantly lower than for direct drive.
Accurate treatments are given by several authors for laser drive and by Hatchett[30] for x-ray drive. Under fusion like conditions, $\dot{M}$ for x-rays is several times higher than for laser light.

On the Nova laser, an extensive series of x-ray driven R-T experiments have been performed[22,27,28]. The x-ray drive used in these experiments was measured by time resolved x-ray filtered photodiode array, with an albedo correction, by the shock break out using a streaked u.v. imager, and by measuring the accelrated foil trajectory using side-on x-ray radiography. These measurements give us confidence in our drive to ~ $\pm$ 5eV.

Perturbation wavelengths from 30μ m to 100μm have been used with various initial amplitudes. By using small initial amplitudes, $a_0(0)$=0.16 μ m, growth

factors up to 75 ± 30 have been observed. For all cases, there is good agreement between the modeling and experiments. As an example, experiments with two different materials, flourosilicone and bromine doped (3% atomic) plastic show excellent agreement with simulations using tabular super-configuration transition array (STA) opacities[31], as illustrated in Fig. 6.

For these experiments, accurate predictions of the evolution of perturbations cannot be made from a simple dispersion relation, because the foil acceleration, which occurs once the shock has transited the foil, is not constant, i.e., the system is not in equilibrium. However to relate the results of code calculations to simple models, an approximate dispersion relation can be obtained at a specific instant in time. For the two different materials used these are shown in Fig. 6. For these drive conditions and for bromine doped plastic at $\lambda = 50$ μm, $\varepsilon = \gamma/(kg)^{1/2} < 0.5$. We conclude from this result, and the many published results, that the R-T growth of the ablation instability in x-ray driven ablation is accurately modeled under these conditions and that adequate reductions of the R-T growth rate can be achieved under conditions with the ablation pressure and wavelengths similar to ignition conditions.

In addition to the single mode experiments, x-ray driven mode coupling experiments have been performed and reported in reference 22. As an example, a foil with two initial wavenumbers $k_1=2\pi$ /50μm and $k_2=2\pi$ /75μm, spawned the sum mode k_1+k_2 (λ =30μm) and the difference mode k_1-k_2 (λ =150μm) once hydrodynamic non-linearity occurred. In reference 22, the agreement between calculations and experiments demonstrates that mode coupling is modeled accurately. The need to consider multi-mode effects when predicting overall perturbation growth is evident.

The model for hydrodynamic instability growth illustrated in Fig. 2 neglects saturation effects in the presence of a full spectrum of 3-D modes. There has been progress in 3-D ablation front instability modeling for test conditions[32], but for x-ray driven experiments the difficulties of 3-D hydrodynamics are compounded with radiation transport. However, experiments can be readily performed and recently 3D bubble and "spike" formation has been measured[22]. Because x-ray drive does not seed imprinting of high k mode structure on the foil, and because the R-T growth rates are relatively low, a very rough initial

surface finish was required for these experiments. With an r.m.s. surface finish of $\sigma = 2\,\mu m$, clear evolution of the spectrum of the perturbations to longer wavelength is seen. Characteristic bubbles and spikes, where the "spikes" become sheets of high density material surrounding the bubbles, are seen. A tendency for the bubbles to become hexagonal, which may be due to a more efficient packing, is evident from the image in reference[22]. Interestingly, 3-D simulations from the Naval Research Laboratory (NRL)[33] of the evolution of full spectrum perturbations from a directly driven foil, show qualitatively similar results.

3.5 Planar directly driven Rayleigh-Taylor experiments

Table 1 lists the laser conditions for recent direct drive experiments on Rayleigh-Taylor instabilitie. The first R-T experiments were performed in the early eighties[25] and were followed by a series of experiments at NRL[34]. These early experiments were not ideal. They were performed at low incident intensity ($\sim 10^{12}$ W/cm^2) and the earlier experiments were without beam smoothing. Moreover the limited laser energy necessitated the use of small focal spots and the experiments were initiated with large perturbations (e.g., 2 μm for 50 μm wavelength) so that mode saturation probably played a major role.

Recently experiments with larger spot sizes, using gated x-ray imaging have more clearly measured small amplitude growth, saturation and laser imprinting[26,37]. In the future, the Nike KrF laser should achieve a 0.25% level of beam smoothness to perform planar experiments. Also the Omega Upgrade laser at the University of Rochester, although designed primarily for implosions, will achieve a 2% smoothness for planar experiments.

A Rayleigh-Taylor experiment with $\lambda = 0.53\,\mu m$ irradiation at 4×10^{13} W/cm^2 has been performed on the Gekko XII laser[36]. In these experiments, the plastic foils had perturbation wavelengths of $\lambda = 30$, 60 and 100 μm, and initial amplitudes 0.3 - 1.0 μm, 0.7-0.8μm and 1.75-2.0 μm respectively. Face on radiography recorded growth factors of up to 10 in areal density in agreement with 2D simulations, although saturation was evident in the experiments. These experiments were most remarkable for the smoothness of the laser beam. The laser amplifiers were driven by broadband amplified spontaneous emission, with

spectral dispersion and phase plates. The resulting time integrated beam profile has a smoothness $\Delta I/I = 2\%$.

In the LLNL experiments[37], a 0.53 μm beam at 0.7×10^{14} W/cm^2 accelerated plastic targets at $g \sim 5 \times 10^{15}$ cm/s^2. Gated x-ray images show the growth and saturation of pre-formed modulations. Good agreement with 2-D calculations is seen for the experiments where the initial amplitudes are large, as shown in Fig. 7. The radiographs show not only the non-linear evolution of the initial modulations but also modulations in areal density, attributable to laser imprinting as discussed below.

A set of initial target amplitude variation experiments on Nova is shown (here τ the opacity is proportional to areal density) in Fig. 8. For an initial amplitude of 0.1 μm, an increase of $\Delta\tau$ of $e^4 \sim 60$ was seen. However, the measured growth rates were below the calculated growth rate for 2-D calculations without imprinting.

Experiments at Nova were also done with smooth foils as shown in Fig. 9. In this case the principal seed perturbations for R-T instability apears to come from structure on the laser beam. The laser beam smoothing technique used on Nova is smoothing by spectral dispersion, where increasing the bandwidth of the laser (0.2 THz to 0.9 THz) causes speckles from the random phase plate to move horizontally as shown in Fig. 9. The face-on radiographs of accelerated foils are shown below the laser beam images. Horizontal patterns, parallel to the grating dispersion direction of the focused laser profiles are evident in the radiographs.

Calculations of the effect of laser seeding on accelerated foils show good agreement with experiments[38]. In the calculations, a model for the laser beam is used to represent the increase in smoothing with time. At early time, the degree of smoothness is poor, causing imprinting by driving modulated shocks through the package. This imprinting is then amplified by the Rayleigh-Taylor instability. The modeling and analysis of the results are performed over a range of modes. However, for simplicity Fig. 10 shows the good agreement for the r.m.s. deviation in opacity vs. time for increasing levels of smoothing. For the LLNL data, the effective initial surface roughness (r.m.s.) that, given a perfectly smooth

beam, would lead to the same degree of modulation of the accelerated target is σ_{eff} ~800Å.

When the effect of this level of laser imprinting is included in the analysis of the growth of pre-modulated packages, the calculated values of $\Delta\tau$ for the 30 μm period of the initial perturbation are lower, as shown in Fig.8. Once this correction is made, there is surprisingly good agreement in the measured growth rate 1.5 ± 0.2 ns^{-1} and the calculated growth rate 1.7 ns^{-1} as shown in table 2 and Fig. 8.

For the small initial amplitude experiments, the ratio $\varepsilon = \gamma/\sqrt{kg}$ is shown in Fig. 11. Over the measured range $\lambda = 20$ μm to $\lambda = 70$ μm, stabilization of $\varepsilon \sim 0.7$ is seen. The Takabe formula is also superimposed on the figure.

This level of stabilization is not adequate for ICF: $\varepsilon < 0.5$ is required (see Sec. II). There are strategies for reducing the growth rate. Verdon in an accompanying paper[21] discusses calculations using shocks to reduce ρ_{max} in Eq 5, thereby increasing v_A. There is a reduction in efficiency of implosions with this strategy although detailed calculations indicate that high gain could still be achieved with ~1MJ of laser energy. An alternative strategy is to use x-rays from high Z dopants in the ablator to reduce ρ_{max}[39]. An old idea[(2)] that is being revisited[40] is to use an oscillating drive to dynamically stabilize a range of wavelengths. Only careful experiments and comparisons with calculations will settle how well these stabilization schemes for direct drive will work.

3.6 Summary and Conclusion

Recent experiments have addressed most of the issues of planar ablation front R-T instability growth. For ICF, there is general agreement that the simplistic arguments that lead to $\gamma / \sqrt{kg} < 0.5$ (for realistic ablation pressure) are correct.

For x-ray drive with ablation pressured close to fusion like conditions, there is good agreement between calculations and experiments on the ablation front instability for perturbation wavelengths in the range 30-100μm conditions. It is shown that $\gamma / \sqrt{kg} < 0.5$ is readily achieved over significant wavelengths.

For direct drive, recent experiments under fusion like conditions have shown good agreement with calculations once the effect of laser imprinting is included. The growth rates are high with $\gamma / \sqrt{kg} \sim 0.7$, but strategies for reducing the growth rate, consistent with implosion efficiency, have been identified. Experiments in the near future will test these strategies.

Future experiments will address other aspects of hydrodynamic instabilities of implosions. Experiments on the inner surface instability have started on the Nova laser and should mature in the near future.

*This work was performed under the auspices of the U.S. Department of Energy by Lawrence Livermore National Laboratory under contract No. W-7405-ENG-48

References

(1) G. Taylor, Proc. Roy. Soc. A 301, 192 (1950): Lord Rayleigh, Proc. Lond. Math. Soc. 14, 170 (1883).

(2) J.P. Boris, Comments on Plasma Physics and Cont. Fusion 3, 1 (1977).

(3) E.A. Frieman, Astrophys. J., 120, 18 (1954).

(4) P. Mulser, Laser & Particle Beam, 6, 118 (1987).

(5) K. Nomoto, T. Shigeyama, Astrophys. J. 368, 27 (1991): S.V. Sarzonov, Planet. Space Sci. 39, 1667 (1991).

(6) S. Zaleski, P. Julien, Tectonophysics 206, 55 (1992).

(7) L.G. Moretto, *et.al.*, Phys. Rev. Lett., 69, 13 (1992).

(8) F.L. Curzon, A. Folkierski, R. Latham and J.A. Nation, Proc. Roy. Soc., 257, 386 (1960).

(9) G. Dimonte, B.A. Remington, and E. Frerking, BAPS 38, 1961 (1993).

(10) B.A. Hammel, BAPS, 38, 2011 (1993).

(11) M.H. Emery, J.H. Gardner, J.P. Boris, Appl. Phys. Lett., 41, 808 (1982). J.D. Lindl and W.E. Mead, Phys. Rev. Lett., 34, 1273 (1975).

(12) S.M. Pollaine, J.D. Lindl, Nuclear Fusion, 26, 1719 (1986)

(13) S.W. Haan Phys. Rev A 39, 5812, (1989).

(14) R.L. McCrory, L. Montierth, R.L. Morse, C.P. Verdon, Phys. Rev. Lett., 46, 333 (1981).

(15) S.E. Bodner, Phys. Rev. Lett. 33, 761 (1974).

(16) J.D.Lindl, private communication, 1982.

(17) R. Betti, C.P. Verdon, R.L. McCrory, Phys. Rev. Lett. in press.

(18) H. Takabe, L. Montierth, R.L. Morse, Phys. Fluids, 26, 2299 (1983): H. Takabe, K. Mima, L. Montierth and R.L. Morse, Phys. Fluids 28, 3676 (1985).

(19) M.H.Emery, J.P.Dahlburg & J.H.Gardner Phys. Fluids 31, 1007 (1987): J.H. Gardner, Phys. Fluids B, 3, 1070, (1991).

(20) M. Tabak, D. Munro & J.D. Lindl, Phys. Fluids B 2,100(1990).

(21) C.P. Verdon, BAPS 38, 2010 (1993); *ibid*, Phys. Fluids B, in press.

(22) B.A. Remington *et.al.*, Phys. Fluids B5, 2589 (1993).

(23) Whitworth, Wark

(24) J.D. Kilkenny, Rev. Sci. Instrum. 63, 4688 (1992).

(25) Cole and Grun

(26) D.K. Bradley *et.al.*, Phys. Rev. Lett. 68 2774 (1992); P.A. Holstein, D. Galmiche & P. Schneider, Nuclear Fusion 32, 667 (1992).

(27) B.A. Remington *et.al.*, Phys. Fluids B4, 967 (1992); *ibid*, Phys. Rev. Lett., 67, 3259 (1991).

(28) J.D. Kilkenny, Phys. Fluids B2, 1400 (1990).

(29) T Af shar-rod, *et.al.*, Central Laser Facility Annual Report, 1993, p. 32.

(30) S. Hatchett, UCRL-JC-108348.

(31) A. Bar-Shalom, J. Oreg, W.H. Goldstein, D. Shvarts, and A. Zigler, Phys. Rev. A. 40, 3183 (1989).

(32) D.L. Youngs, Phys. Fluids A3, 1312 (1991); J.P. Dahlburg and J.H. Gardner, Phys. Rev. A. 41, 5695 (1990); H. Sakagami and K. Nishimura, Phys. Rev. Lett., 65, 432 (1990).

(33) J.P. Dahlburg, J.H. Gardner, D.E. Fyfe and S.W. Haan, BAPS 38, 1962 (1993).

(34) J. Grun *et.al.*, Phys. Rev. Lett. 58, 2672 (1987) and references therein. J. Grun, M.E. Emery, C.K. Manka, T.N. Lee, E.A. McLean, A. Mostovych, J.

Stamper, S.E. Bodner, S.P. Obenschain, and B.H. Ripin, Phys. Rev. Lett. 58, 2672 (1987).

(35) M. Desselbeger and O. Willi, Phys. Fluids B 5, 896 (1993).

(36) M. Katayama, H. Azechi, A. Nishiguchi, M. Nakai, S. Nakai, ILE Quarterly Progress Report, 43, 27 (1992).

(37) S.G. Glendinning *et.al.*, Phys. Rev. Lett., 69, 1201 (1992).

(38) S. Weber, ICF Quarterly Report 2, 172 (1992),UCRL-LR-105821-92-4.

(39) J.P. Knauer, BAPS 38, 1961 (1993).

(40) R. Betti, BAPS 37,1470 (1992).

Figure Captions.

Fig. 1. The Rayleigh-Taylor instability (left) has eigenmodes $(\cos kx)e^{-kz}$ where $k=2\pi/\lambda$. The flow lines are approximated as a manometer (center). The stability of a manometer with high density fluid on top can be represented by a compound pendulum (right), with a heavy mass ρ_{hi} above and a lighter mass ρ_{lo} below.

Fig. 2. Illustration of: (1) The ablation front Rayleigh-Taylor instability growth from surface noise or laser seeded areal density modulations, (2) the shell feed through to seed inner surface perturbations and (3) the Rayleigh-Taylor growth of seeded inner surface perturbations during the deceleration of the shell.

Fig. 3. Calculated density, pressure and velocity profiles for $\lambda=0.26\mu m$ irradiation at $2\ 10^{14}$ W/cm^2 of a plastic foil. The unstable region where $\nabla p.\ \nabla\rho$ is negatiive is also shown. The average velocity in this region is $\sim 2 \times v_A$ where v_A is the flow velocity at ρ_{max}.

Fig. 4. Calculations of the reduction in the R-T growth rate for direct drive (left) and indirect drive (right). The direct drive calculations are from Tabak[20] and Gardner[19] at 2 and 3 10^{14} W/cm^2 respectively for $\lambda=0.26\ \mu m$ drive. The lower curve for direct drive is for an artificially increased (4x) isentrope. The graph on the right is for x-ray drive and for two different materials, fluorosilicone and brominated plastic and similar drive conditions as above.

Fig. 5 Side-on radiography (upper) has been used to measure the growth of modulations, but requires planar targets, good temporal and spatial resolution, and because of the large areal density, high photon energy. Face-on radiography (lower) only requires spatial resolution $<\lambda$.

Fig. 6 Medium initial amplitude experiments (left) for pulsed shaped x-ray drive of flourosilicone and brominated plastic, showing excellent agreement with calculations. The calculations are made to fit a simple dispersion relation with the calculated values of L and v_A and an adjustable parameter β which is in the range 1.5-2.5. For $\lambda < 100\ \mu m$ $\varepsilon = \gamma/\sqrt{kg} < 0.5$, demonstrating adequate ablative stabilization.

Fig. 7 Direct drive results from premodulated targets with large initial modulations, showing the non-linear formation of bubbles and spikes.

Fig. 8 Measured growth of ln ($\Delta\tau$) for targets with initial amplitudes $a_o(0)$ of 0.1 and 0.2 μm. There is a point at time t=0 for both cases, measured from the initial target characterization.

Fig. 9 The time averaged modulations in the laser power (upper) and time gated radiographs of accelerated packages (lower) with increasing laser smoothing 0, 0.2THz and 0.9THz. The pattern of modulations of the radiographs with horizontal streaks resembles the modulations in the laser, except that the short wavelength structure of the laser is smoothed.

Fig. 10 R.m.s. deviation in optical depth due to laser imprinting for modeling and the experiment. The effect of increased smoothing on the modulations in areal density as the laser bandwidth is increased, is evident. Good agreement with experiments is seen.

Fig. 11 The measured growth rates for the LLNL experiments, normalized to the classical growth rates for λ=0.53μm drive at 7×10^{13} W/cm^2. For these experiments inadequate ablative stabilization is seen.

	Early Glass (Rutherford NRL)	Rutherford Appleton	LLNL	Osaka	*Planned* *LLE*	*NRL(KrF)*
I W/cm^2	*5 10^{12}-10^{13}*	1.5 10^{14}	0.7 10^{14}	0.7 10^{14}	*2 10^{14}*	*2 10^{14}*
λ (μm)	*1, 0.53*	0.53	0.53, 0.35	0.53	*0.35*	*0.26*
Beam Smoothness $\delta I/I$ ($t=\infty$)	*30-10%*	7%	8%	2%	*2%*	*.25%*
pulse shaping	*no*	no	yes	partial	*yes*	*yes*

Table 1

a_0 μm	Growth rate (simulated) ns^{-1}	Growth rate (experiment) ns^{-1}
0.25	1.6	1.5±0.2
0.1	1.7	1.5±0.2

Table 2

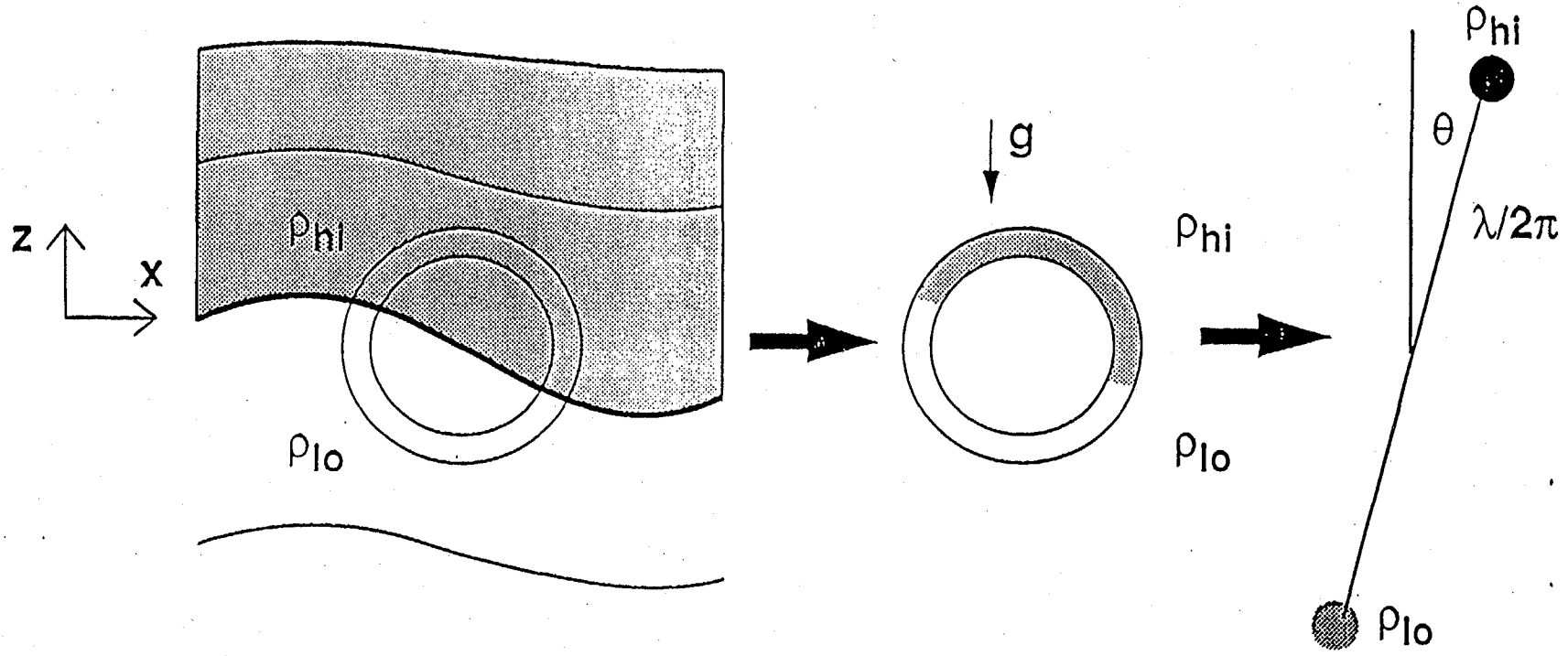

Fig. 1

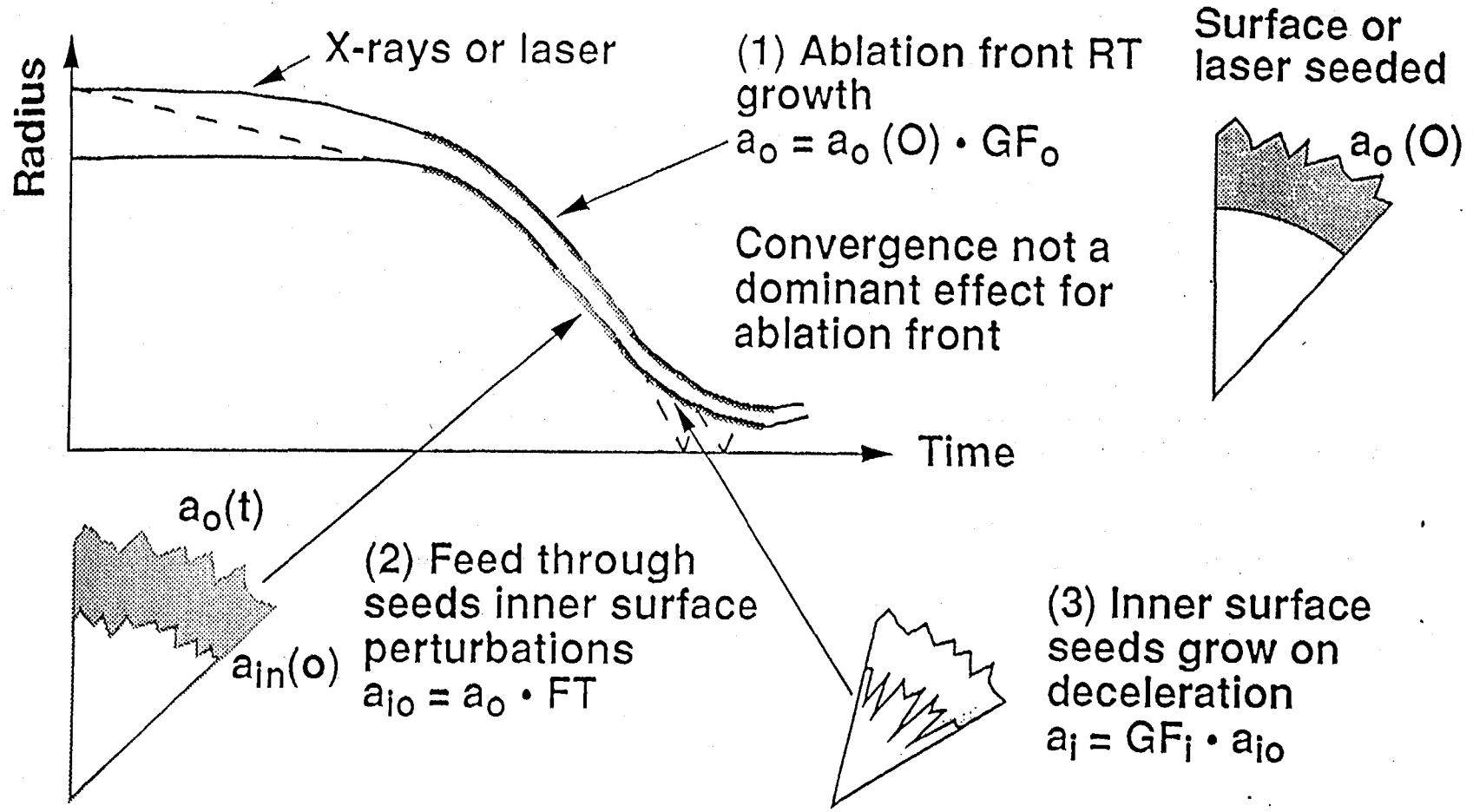
Radius
X-rays or laser
(1) Ablation front RT growth
$a_o = a_o(O) \cdot GF_o$
Convergence not a dominant effect for ablation front
Surface or laser seeded
$a_o(O)$
Time
$a_o(t)$
$a_{in}(o)$
(2) Feed through seeds inner surface perturbations
$a_{io} = a_o \cdot FT$
(3) Inner surface seeds grow on deceleration
$a_i = GF_i \cdot a_{io}$

Fig. 2

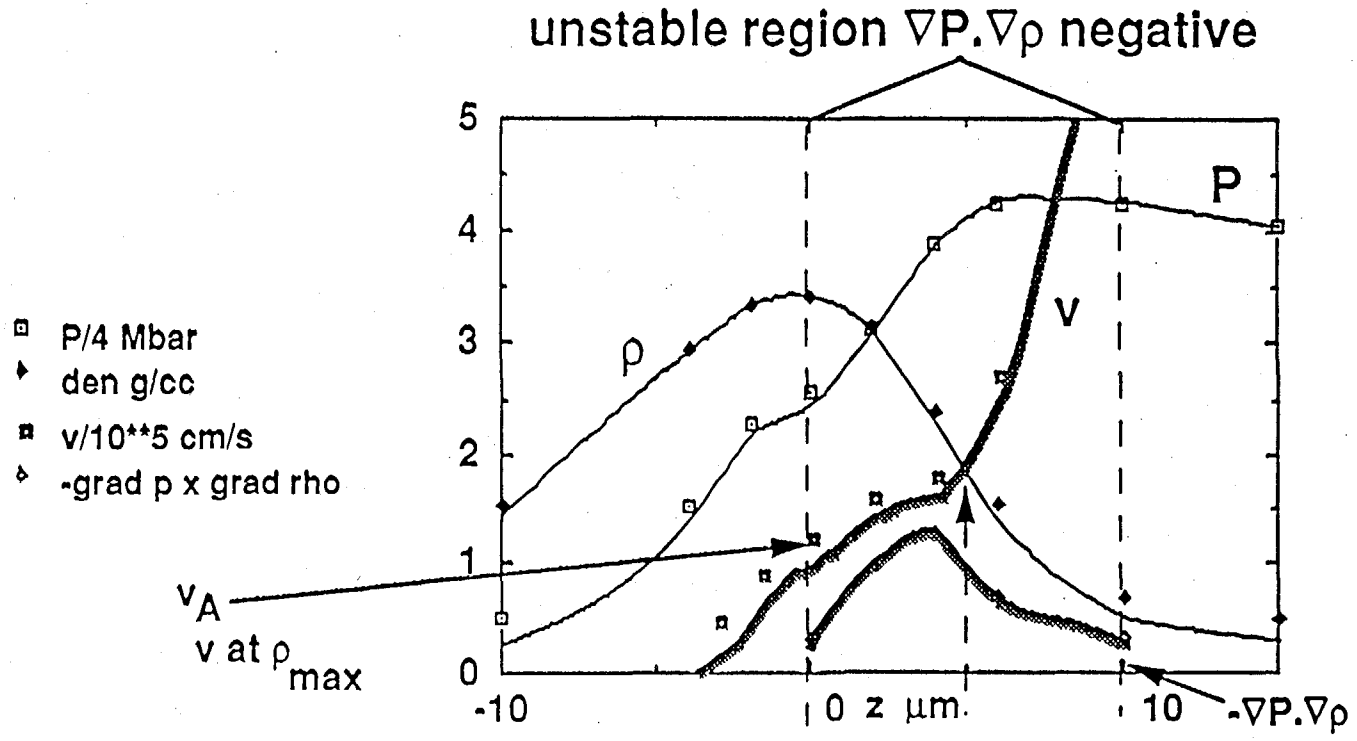
unstable region ∇P.∇ρ negative
P/4 Mbar
den g/cc
v/10**5 cm/s
-grad p x grad rho
5
4
3
2
1
0
-10
0 z μm
10
P
ρ
v
v_A
v at ρ_{max}
-∇P.∇ρ

Fig. 3

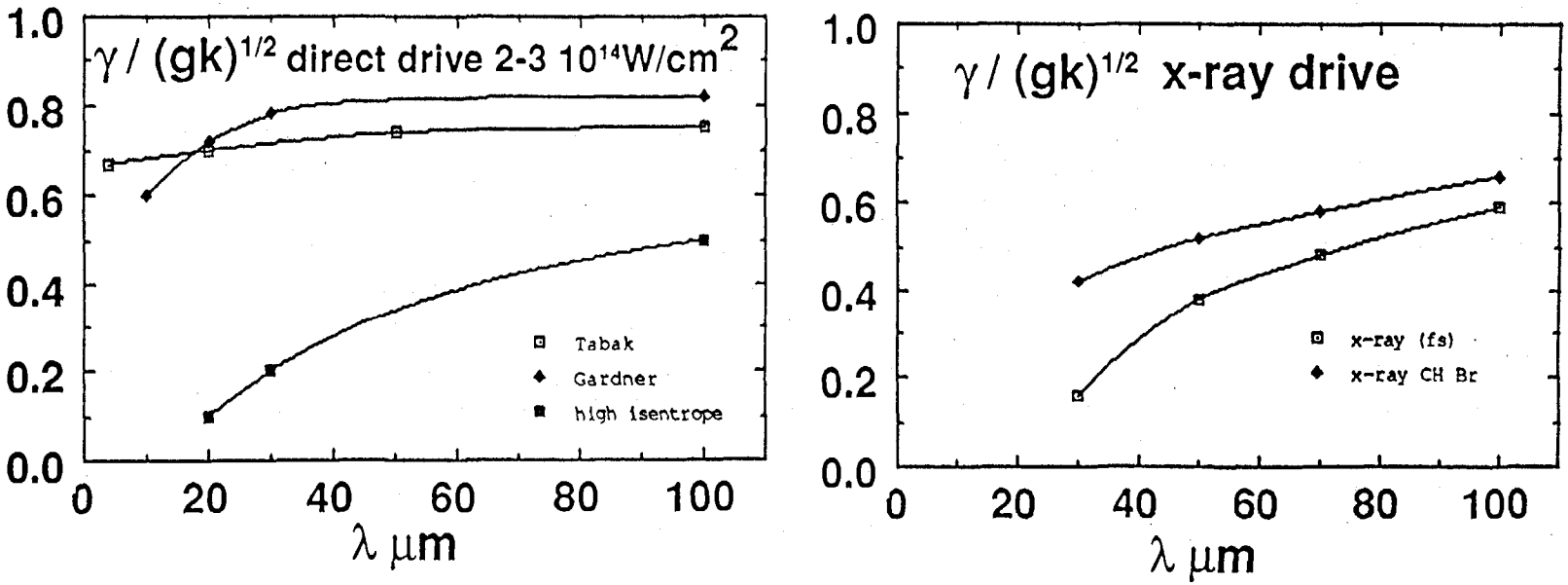
1.0
0.8
0.6
0.4
0.2
0.0
γ / (gk)^1/2 direct drive 2-3 10^14W/cm^2
Tabak
Gardner
high isentrope
0
20
40
60
80
100
λ μm
1.0
0.8
0.6
0.4
0.2
0.0
γ / (gk)^1/2 x-ray drive
x-ray (fs)
x-ray CH Br
0
20
40
60
80
100
λ μm

Fig. 4

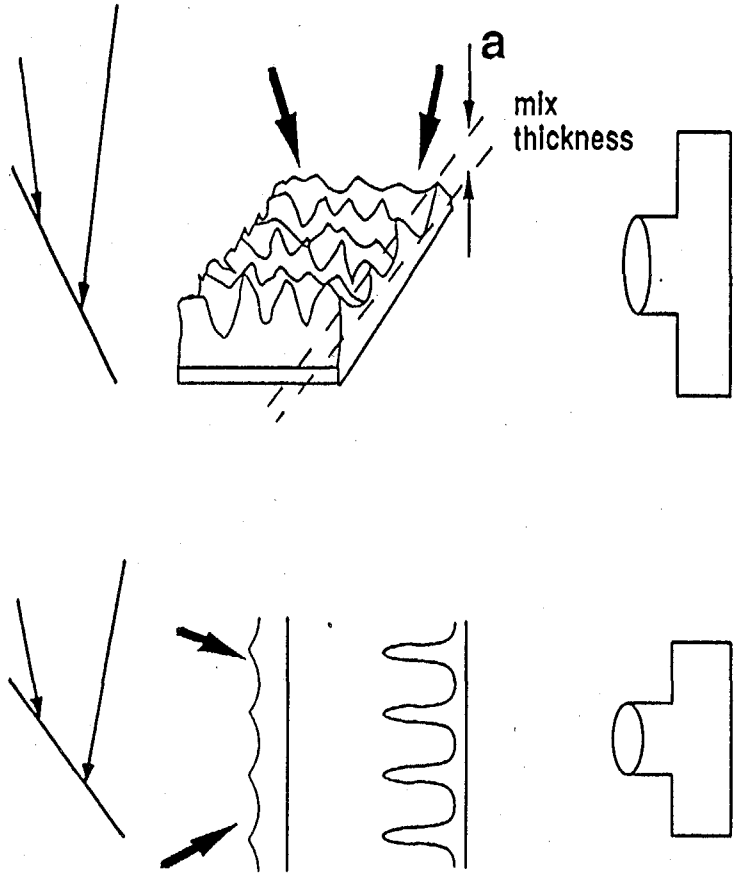

Fig. 5

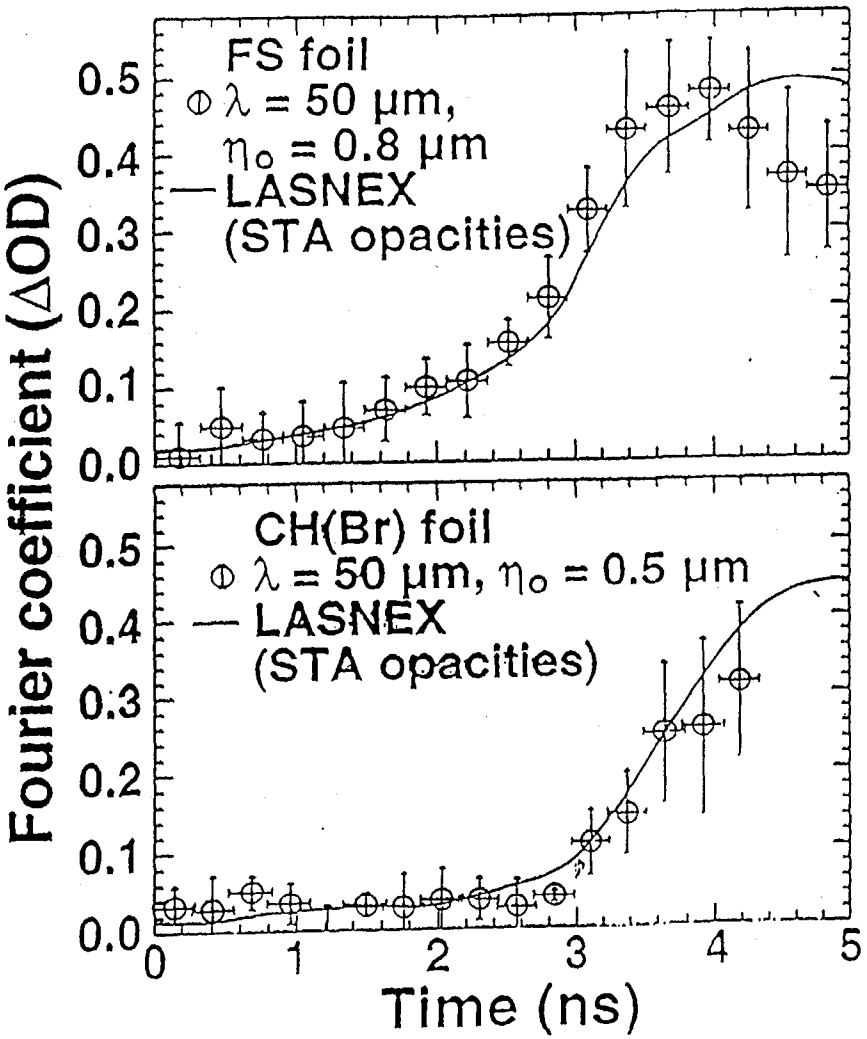

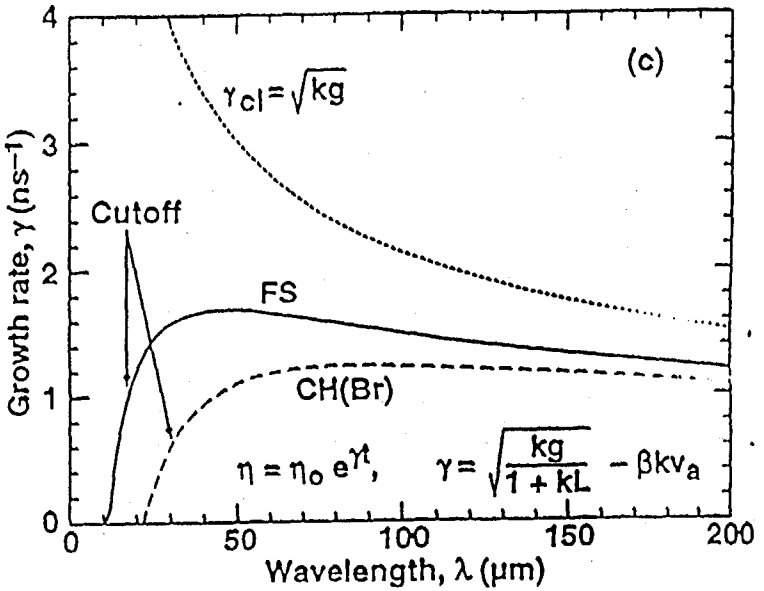

$g = 7 \times 10^{15}$ cm/s², FS (CH(Br)):
$v_a = 3.2\ (3.9) \times 10^5$ cm/s,
$L = 1.6\ (4.0)$ μm,

Fig. 6

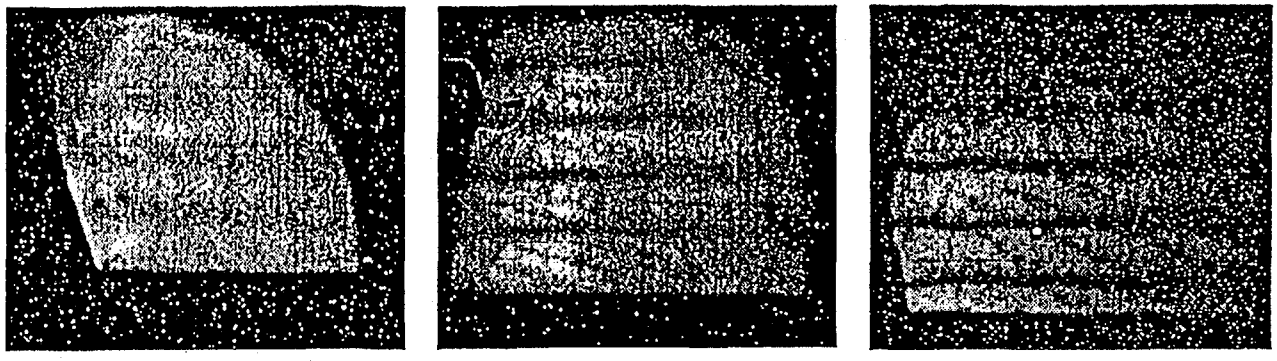

t=1.2 ns t=2.0 ns t=2.8 ns

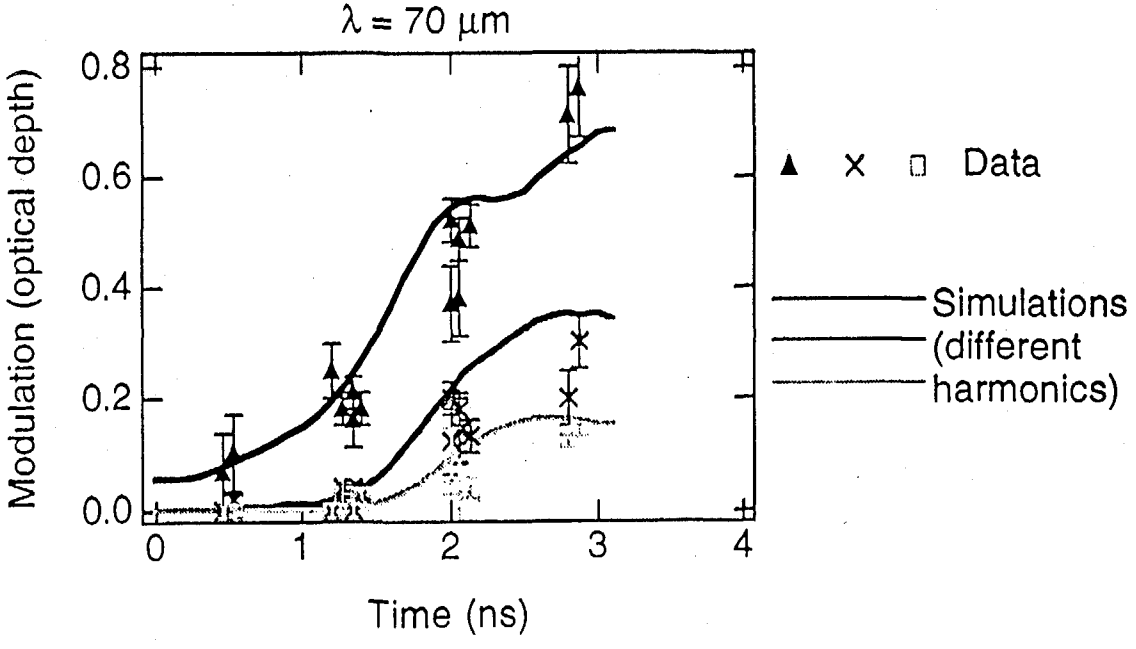

Fig. 7

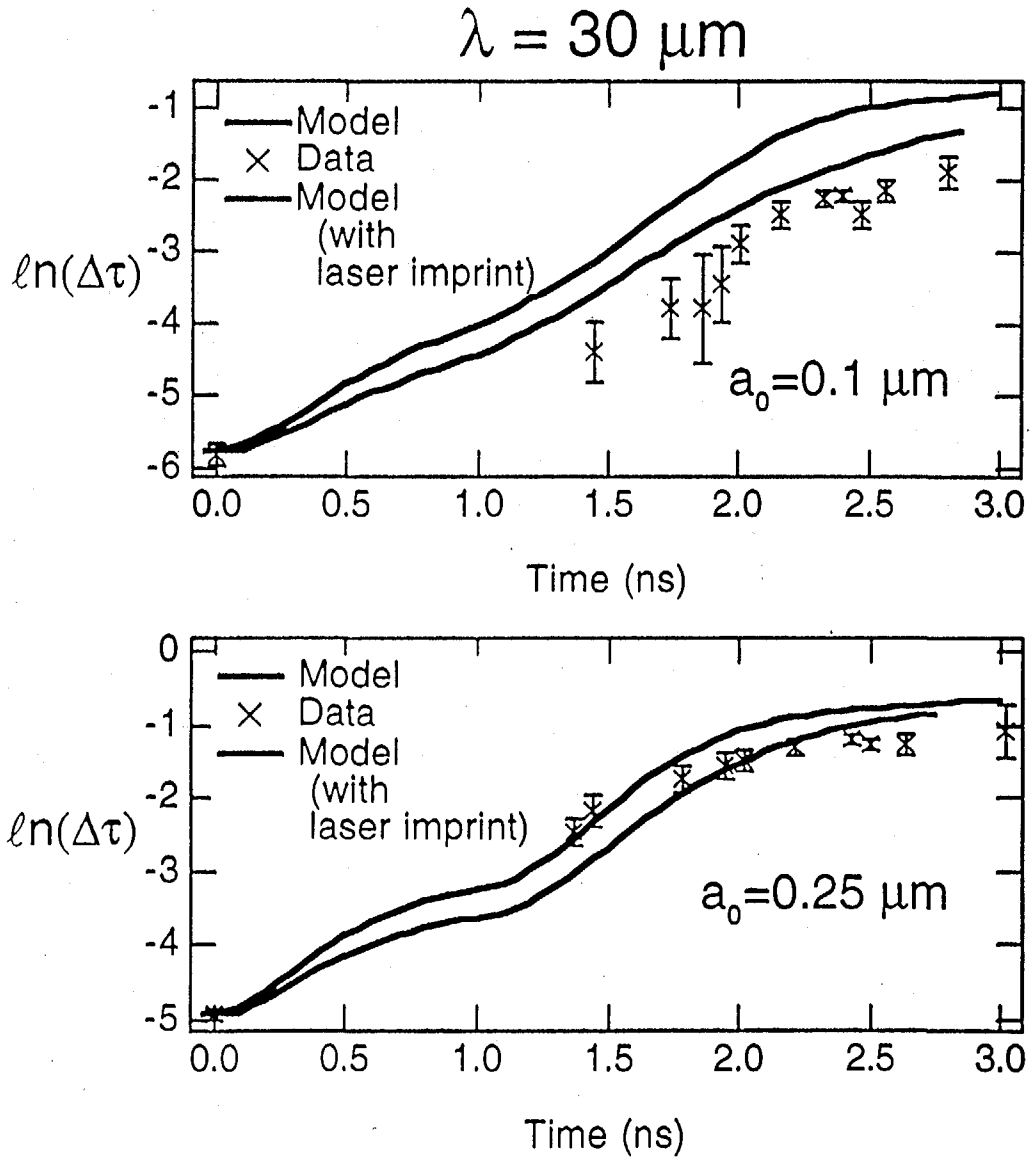
λ = 30 μm
Model
Data
Model
(with
laser imprint)
a0=0.1 μm
ℓn(Δτ)
-1
-2
-3
-4
-5
-6
0.0
0.5
1.0
1.5
2.0
2.5
3.0
Time (ns)
Model
Data
Model
(with
laser imprint)
a0=0.25 μm
ℓn(Δτ)
0
-1
-2
-3
-4
-5
0.0
0.5
1.0
1.5
2.0
2.5
3.0
Time (ns)

Fig. 8

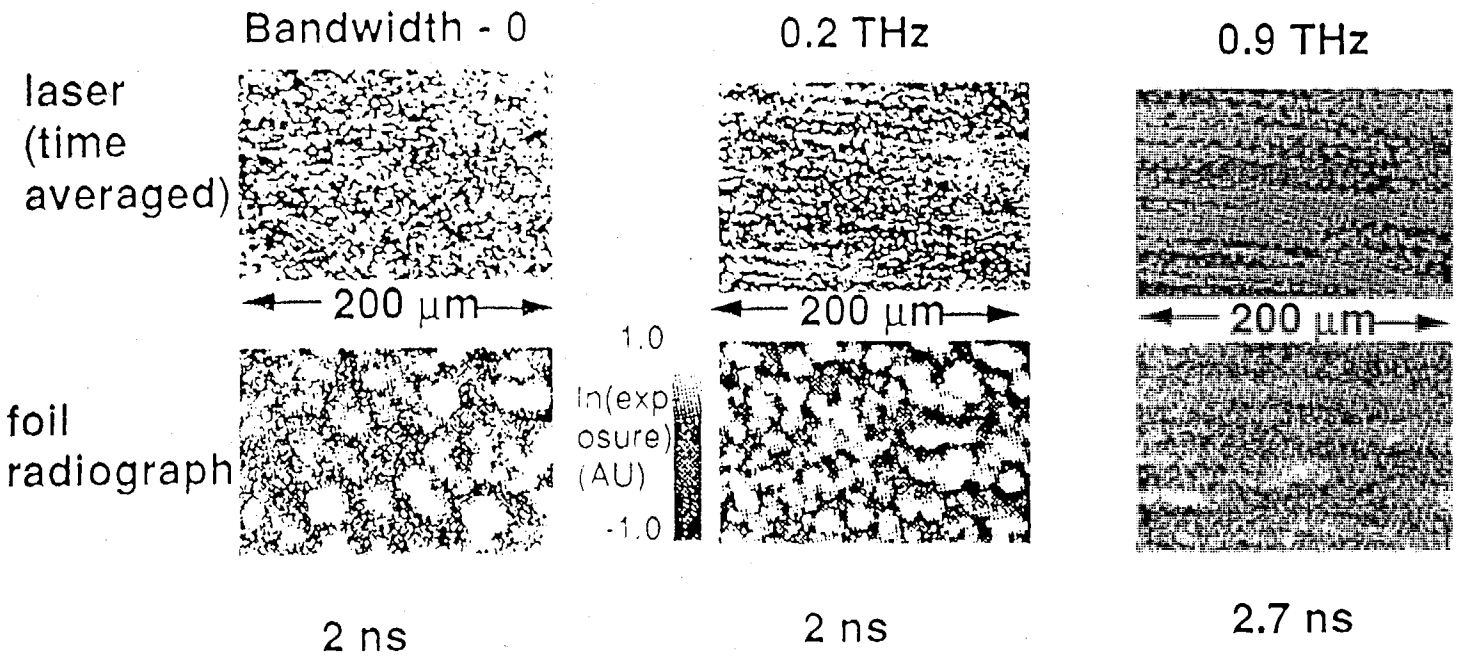
Bandwidth - 0
0.2 THz
0.9 THz
laser
(time
averaged)
200 μm
200 μm
200 μm
foil
radiograph
1.0
ln(exp
osure)
(AU)
-1.0
2 ns
2 ns
2.7 ns

Fig. 9

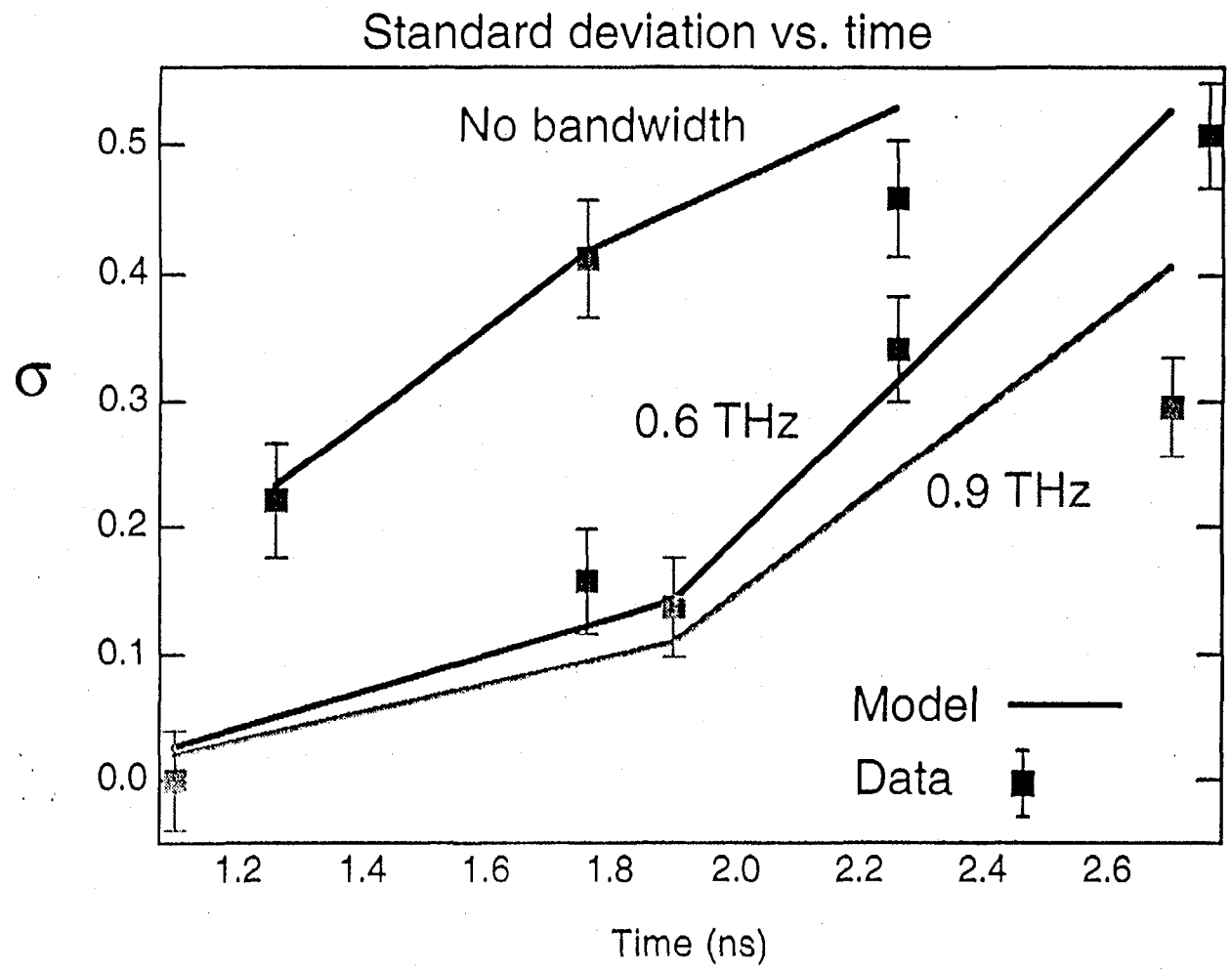
Standard deviation vs. time
No bandwidth
0.6 THz
0.9 THz
Model
Data
σ
0.0
0.1
0.2
0.3
0.4
0.5
1.2
1.4
1.6
1.8
2.0
2.2
2.4
2.6
Time (ns)

Fig. 10

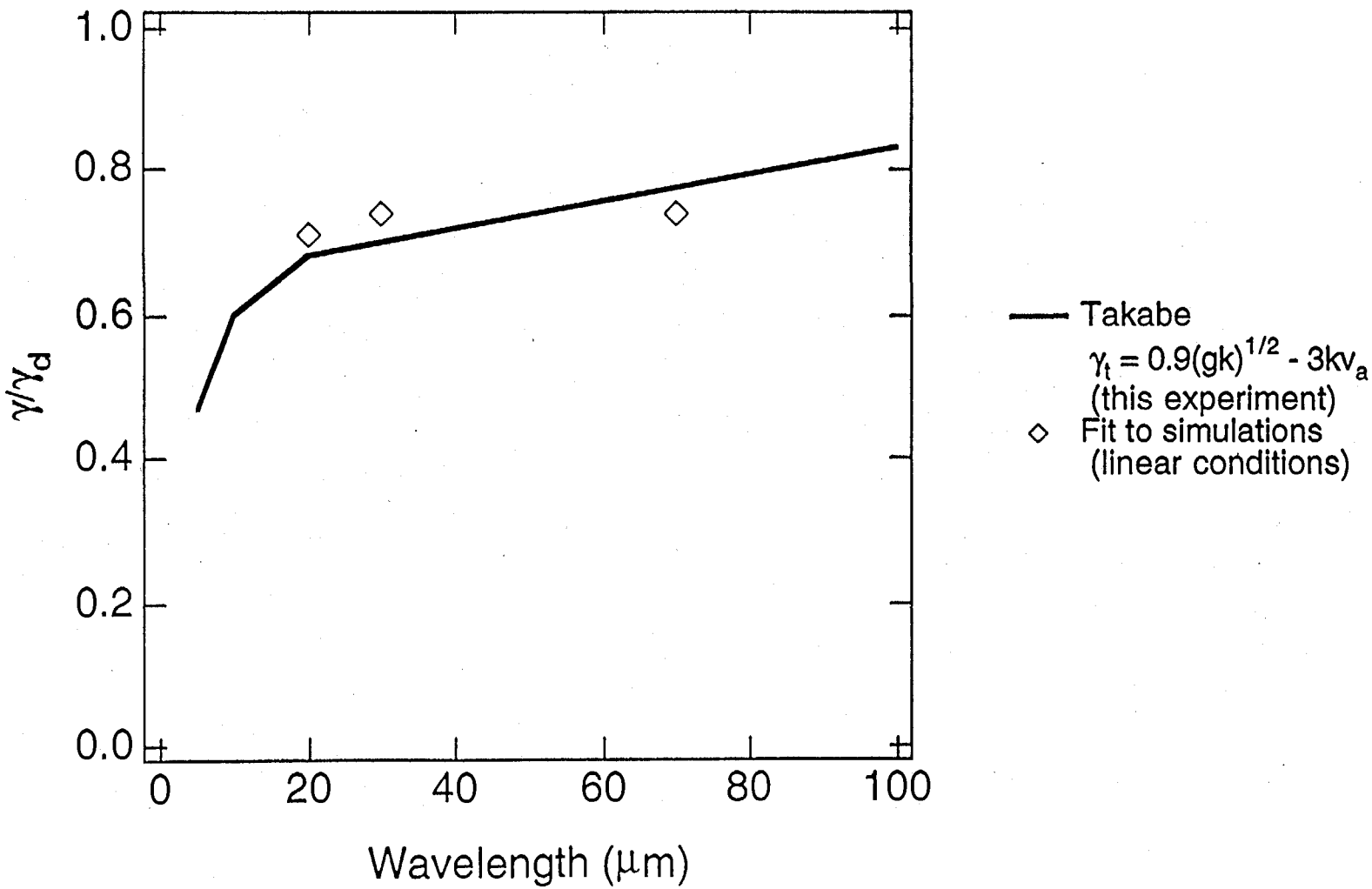
1.0
0.8
0.6
0.4
0.2
0.0
γ/γ_d
0
20
40
60
80
100
Wavelength (μm)
Takabe
$\gamma_t = 0.9(gk)^{1/2} - 3kv_a$
(this experiment)
Fit to simulations
(linear conditions)

Fig. 11